# MATERIAL PARAMETERS OF CEMENT AND ALKALI ACTIVATED FLY ASH BASED CONCRETE: LABORATORY MEASUREMENTS AND NUMERICAL SIMULATION

Michal Šejnoha*, Miroslav Brouček*, Eva Novotná*
Zbyněk Keršner**, David Lehký**, Petr Frantík**

*The paper reports on the determination of basic mechanical material parameters of several concrete and alkali activated concrete and fly ash mixtures intended for the construction of segmental lining used in TBM tunneling. The results of an extensive experimental program are discussed first. The principal attention is accorded to the experimental determination of specific fracture energy from a load-deflection curve, which, when compared to numerical simulations, shows certain inconsistency with the measurements of other material data. This is supported by the derivation of the data from inverse analysis employing the elements of soft computing. Dynamic simulation of crack propagation experiments is suggested to reconcile the essential differences and to identify the most important impacts affecting the results of experimental measurements.*

Keywords: *alkali activated fly ash, concrete, fracture energy, finite element simulation, soft computing*

## 1. Introduction

Massive increase of $CO_2$ emission in recent years has supported a considerable effort towards substitution of ordinary Portland cement by alkali-activated aluminosilicate materials such as fly ash in the production of concrete. Using fly ash as admixture in cements is now common in many applications. Full substitution for large scale structural units, however, is still at its infancy and to foster its progress beyond laboratory samples will require fundamental understanding of what is occurring already on the level of paste during alkali-activation process. Starting with recent accomplishments by [1] we expect considerable activity in this field in the coming decade.

This topic, however, goes beyond the present scope. Instead we focus our attention on the macroscopic evaluation of the response of various specimens of mixtures of concrete and alkali-activated materials with emphases on the influence of fly ash replacing either a certain portion or an entire amount of cement. We report on both experimental and numerical part of this research effort as these should be considered on the same footing to mutually corroborate the obtained results.

* prof. Ing. M. Šejnoha, Ph.D., DSc., Ing. M. Brouček, Ph.D., Ing. E. Novotná, Ph.D., Czech Technical University in Prague, Faculty of Civil Engineering, Thákurova 7; 166 29, Prague; CZ
** prof. Ing. Z. Keršner, CSc., Ing. D. Lehký, Ph.D., Ing. P. Frantík, Ph.D., Brno University of Technology, Faculty of Civil Engineering Veveří 331/95 602 00 Brno; CZ

Motivated by possible applications of these mixtures in the production of the segments of lining often used in hostile environment we set up an extensive experimental program that includes on the one hand small scale laboratory measurements of basic material parameters, material degradation due to activity of acid solutions, and on the other hand full scale measurements of resistance of lining segments to fire.

The present contribution is limited to the first part of this program (small scale testing) aiming at quantification of individual mixtures with regard to their mechanical material data in the light of the required strength corresponding to concrete C50/60 and their durability. The results of numerical simulations of selected tests are also present to warn engineers against blindly accepting the provided laboratory data which might not be suitable for intended numerical analysis on a structural level.

The remainder of this paper is organized as follows. Section 2 provides the list of examined mixtures. The results of experimental investigation are summarized in Section 3. Numerical part embracing also the identification of material parameters based on fracture energy measurements is described in Section 4. Brief summary is finally given in Section 5.

## 2. Concrete and alkali activated mixtures

We begin by providing the list of examined concrete and alkali activated mixtures. Eight mixtures in overall were proposed. Two mixtures in particular assumed total replacement of concrete by fly ash activated by strong alkaline liquids such as a mixture of NaOH pellets dissolved in tap water and sodium silicate in the form of water glass. Low-calcium fly ash coming from the Mělník (FAM) and Opatovice (FAO) thermal electric power plants was used. Half the mixtures were further modified by adding 0.5 % of volume of synthetic fibers Forta-Ferro. This amounted to 4.5 kg of fibers per 1 $m^3$ of the mixture.

The following notation is introduced to distinguish individual mixtures: C – cement based concrete (reference mixture), POP – alkali-activate fly ash, Fi – mixture containing fibers, FAC-1(2) – mixtures with partial replacement of cement by fly-ash. All the mixtures considered the same grading curve. Specific fractions of stone grains are listed in Table 1. Composition of individual mixtures is then presented in Table 2.

| Fraction | Amount per 1 $m^3$ of mixture in [kg] |
|---|---|
| 0/4 | 705 |
| 3/8 | 130 |
| 8/16 | 865 |

*Tab.1: Fraction of grains*

| Material | Amount per 1 $m^3$ of mixture in [kg] | | | |
|---|---|---|---|---|
| Mixture → | C | FAC-1 | FAC-2 | POP |
| CEM I 52,5 R | 460 | 322 | 322 | – |
| Limestone powder | 40 | 40 | 40 | – |
| Water | 150 | 150 | 187 | 51 |
| Fly ash | | 138 (FAM) | 276 (FAM) | 400 (FAO) |
| NaOH | – | – | – | 29,4 |
| Water glass 34% | – | – | – | 127,5 |
| Slaked lime | – | – | – | 12 |
| Glenium ACE | 4.2 | 4.2 | 4.2 | 12 |

*Tab.2: List of selected mixtures*

It will be seen in the next section that all samples of cement based mixtures exceeded the required compressive strength of 50 MPa. Inability of alkali-activated mixtures (POP, FiPOP) to reach this value can be attributed to the insufficient curing temperature of about 40−45 °C. Typically, the curing temperature of such composites amounts to about 65−80 °C to sufficiently accelerate the hydration process. However, such conditions would create an insuperable obstacle for mass production.

## 3. Experimental program

Standard laboratory measurements were carried out at the Klokner Institute in Prague to obtain elastic moduli, cubic and prism compressive strength, strength in transverse tension and specific fracture energy of individual mixtures. The particular results are reported in the sequel.

### 3.1. Specific fracture energy

First, our attention was dedicated to the determination of fracture energy from a three-point bending test displayed in Fig. 1(c). Three notched specimens for each mixture having dimensions 150×150×700 mm with a notch depth of 25 mm, see Fig. 1(a), were tested in a displacement-controlled loading regime at the rate of 0.05 mm/min up to 0.2 mm of crack mouth opening displacement (CMOD) and at the rate of 0.2 mm/min from 0.2 mm until failure. Both the specimen size and loading rate were selected such as to comply with the general recommendations provided by [13] concerning the size of the largest aggregate, recall Table 1, and the time to reach the peak load.

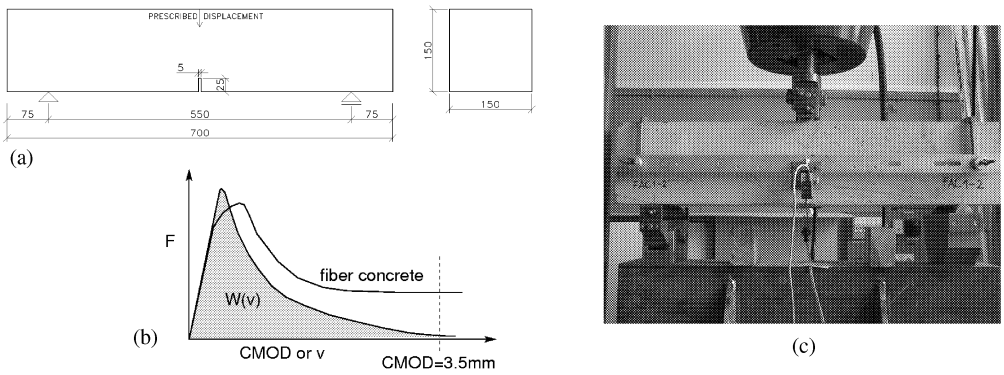


*Fig.1: Three-point bending test: (a) Computational scheme, (b) Example of loading curve, (c) Experimental set-up*

A rather stiff loading machine MTS 500 kN was used to perform the measurements. As seen from Fig. 1(c) the vertical displacement $v$ of a central point was recorded with respected to the line connecting two other points located on the beam above the supports. All measurements were performed 28 days since the time of their production. For standard specimens without fibers the formula provided by [12] was adopted to evaluate the specific fracture energy $G_{\mathrm{f}}$

$$G_{\mathrm{f}} = \frac{W + m\,g\,v_{\max}}{A_{\mathrm{lig}}}\,, \tag{1}$$

where $A_{\text{lig}}$ is the projected fracture area, $m\,g$ is the specimen weight, $v_{\max}$ is the maximum vertical deflection at failure and $W$ represents the area under the $F-v$ loading curve, see Fig. 1(b). In the present study it was evaluated using a simple trapezoidal rule in the form

$$W = \sum_{i=1}^{N} F_i\,\Delta v_i\ , \tag{2}$$

where $\Delta v_i$ is the increment of maximum vertical deflection between two recorded measurements $i-1$ and $i$, $F_i$ is the corresponding average force and $N$ is the total number of measurements. Since having only a minor effect on the final value, the second term in the brackets of Eq. (1) was neglected. As for the fibrous specimens the same formula was used assuming $v_{\max}$ that corresponds to CMOD = 3.5 mm as schematically plotted in Fig. 1(b).

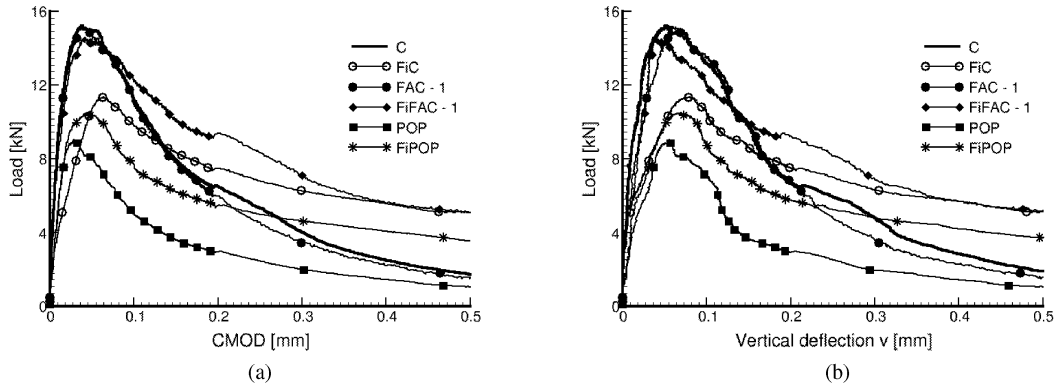


*Fig.2: Selected loading diagrams: (a) $F-$CMOD, (b) $F-v$*

Averages calculated for individual mixtures are available in the last column of Table 3. Some representatives of the loading curve are plotted in Fig. 2 showing a relatively large residual strength up to 30 % of the peak value for specimens containing fibers. Fig. 3(a) plots the distribution of the rate of CMOD as a function of time suggesting, primarily due to high stiffness of the loading machine, no loss of stability during the test. A certain jump in the original trend is attributed to the change of the loading rate well after exceeding the peak load to accelerate the course of measurements. The issue of loss of stability in the displacement control loading is well described in [9].

Smaller values of specific fracture energy, being in accord with small ultimate strength, of alkali activated fly ash based specimens in comparison to concrete specimens can be blamed on an uneven distribution of stone aggregates within the sample as seen from plots of fracture surfaces in Fig. 3(c). This is primarily attributed to non-optimal composition, in particular the amount of water, which was kept comparable to other mixtures. Modifications are currently under way to avoid such an undesirable feature.

### 3.2. Young's modulus and strength parameters

While cubic specimens having edge length of 150 mm were used to measure strength properties ($f_{\text{c,cube}}$, $f_{\text{t}}$), 300×150×150 mm prisms were adopted to acquire the values of Young's moduli. These specimens were further utilized to provide the uniaxial compressive

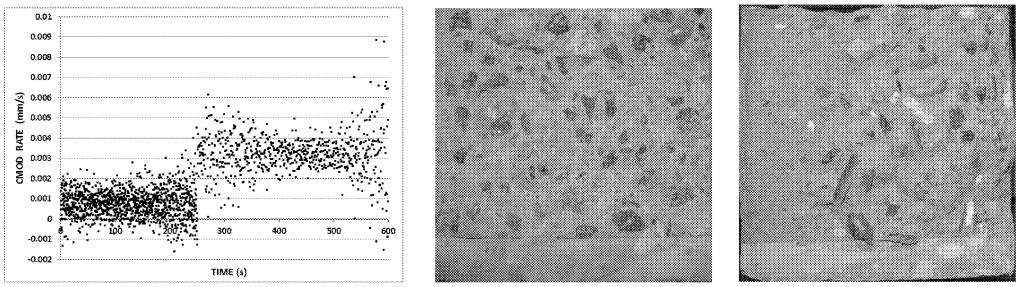


(a) (b) (c)

*Fig.3: (a) Rate of CMOD; Fracture surfaces: (b) Concrete specimen, (c) Alkali activated fly ash specimen*

| Notation | Elastic modulus | Compressive strength | Transverse tension strength | Fracture energy |
|---|---|---|---|---|
| | $E$ [GPa] | $f_{\mathrm{c,cube}}$ / $f_{\mathrm{c,prism}}$ [MPa] | $f_{\mathrm{t}}$ [MPa] | $G_{\mathrm{f}}$ [N/m] |
| C | 38.5 | 84.7 ($96^{+}$) / 72 | 4.4 | 207.4<br>220.3, 190.3 |
| FiC | 39.5 | 78.0 ($76^{+}$) / 65 | 3.7 | 950.5 |
| FAC-1 | 40.1 | 66.3 ($89^{+}$) / 59 | 3.1 | 190.9 |
| FiFAC-1 | 39.7 | 61.3 ($88.8^{+}$) / 63 | 3.1 | 819 |
| FAC-2 | – | $54.0^{*}$ ($71.0^{**}$) | – | – |
| FiFAC-2 | – | $48.2^{*}$ ($69.9^{**}$) | – | – |
| POP | 18.9 | 36.2 / 28 | 2.9 | 112.3 |
| FiPOP | 20 | 39.5 ($40.4^{+}$) / 30 | 2.9 | 882.5 |

*Tab.3: Material properties of samples tested after* 28, 60 *(∗)*, 180 *(∗∗) and* 450 *(+) days of curing*

strength $f_{\mathrm{c,prism}}$. All specimens were cut from undamaged remainders of the fractured specimens. This ensured that the same material compositions as used in the fracture tests were examined. The results appear in Table 3.

To address the expected pozzolanic reaction the samples corresponding to mixtures FAC-2 and FiFAC-2 with increased amount of fly ash were tested after 60 (∗) and 180 (∗∗) days of curing. The measured values of cubic strength confirm the ongoing pozzolanic reaction even without alkaline activators. Unfortunately, the applicability of structural elements made from these mixtures might be limited by low strength at early time of curing. Selected mixtures were yet tested after 450 (+) days also supporting the previous remark at least for concrete specimens. On the contrary, further increase of compressive strength of alkali activated fly ash based mixtures over the time has not been observed.

### 3.3. Influence of corrosive environment

This particular experiment serves to address a potential influence of a long term action of aggressive ground water on mechanical properties of examined mixtures. Following the discussion with experts in tunnel construction we chose a sulphate solution as the decisive element in evaluating the resistivity of a tunnel lining. A dynamic modulus of elasticity is adopted here to verify the potential material degradation. The measurements were carried out with the help of a non-destructive ultrasound method on cubic 150×150 mm specimens. The MATEST Ultrasonic tester (palmer 'High Technology' with microprocessor for

combined ultrasonic and rebound hammer data acquisition and processing C372N) was employed to determine the time of wave propagation. The dynamic modulus of elasticity $E_{\mathrm{DYN}}$ then follows from

$$E_{\mathrm{DYN}} = \rho \frac{\frac{L^2}{T}}{k^2} , \tag{3}$$

where $\rho$ is the bulk weight of the material, $L$ and $T$ represent the length of a measuring base and an average time of wave propagation, respectively, and $k$ is the coefficient depending on the relation of $L$ and $T$ attaining the value of either 1 or 1.0541 .

Since this is an ongoing experiment, we report only the results collected in a relatively short period of 11 months for concrete specimens and 7 months for alkali activated fly ash based mixtures. Table 4 lists the actual values of dynamic moduli for a particular period of time. Note that the initial value corresponds to dry conditions. This value typically increases upon soaking the specimen into a liquid solution, which explains the initial increase of this value measured after 4 months. An onset of degradation process, although at a very slow rate, can be observed when comparing the initial values with those corresponding to time period of 11 months. Taking the change of $E_{\mathrm{DYN}}$ in water as a reference value equal to zero, we may evaluate the influence of aggressive solution upon plotting the change of $E_{\mathrm{DYN}}$ for a given solution with respect to this reference value. The results appear in Fig. 4.

| Mixture | Solution | Initial value | After 4 months | After 11 months (After 7 months) |
|---|---|---|---|---|
| C | $H_2O$ | 53.7 | 58.9 | 57.7 |
| C | $Na_2SO_4$ | 55.4 | 61.7 | 58.9 |
| C | $Mg_2SO_4$ | 54.0 | 61.0 | 60.8 |
| FiC | $H_2O$ | 53.6 | 59.8 | 59.5 |
| FiC | $Na_2SO_4$ | 53.2 | 58.7 | 57.0 |
| FiC | $Mg_2SO_4$ | 50.2 | 58.4 | 57.5 |
| FAC-1 | $H_2O$ | 52.2 | 61.1 | 55.6 |
| FAC-1 | $Na_2SO_4$ | 52.0 | 57.5 | 57.1 |
| FAC-1 | $Mg_2SO_4$ | 52.2 | 59.6 | 59.5 |
| FiFAC-1 | $H_2O$ | 51.0 | 57.9 | 56.2 |
| FiFAC-1 | $Na_2SO_4$ | 49.3 | 57.7 | 56.8 |
| FiFAC-1 | $Mg_2SO_4$ | 50.8 | 57.6 | 56.9 |
| FAC-2 | $H_2O$ | 47.0 | 52.6 | 52.1 |
| FAC-2 | $Na_2SO_4$ | 49.3 | 54.4 | 54.2 |
| FAC-2 | $Mg_2SO_4$ | 47.6 | 54.3 | 53.1 |
| FiFAC-2 | $H_2O$ | 48.5 | 52.5 | 52.4 |
| FiFAC-2 | $Na_2SO_4$ | 47.4 | 53.4 | 52.5 |
| FiFAC-2 | $Mg_2SO_4$ | 47.3 | 54.4 | 53.6 |
| POP | $H_2O$ | 28.7 | - | (35.9) |
| POP | $Na_2SO_4$ | 28.3 | - | (33.5) |
| POP | $Mg_2SO_4$ | 30.1 | - | (36.5) |
| FiPOP | $H_2O$ | 25.6 | - | (31.5) |
| FiPOP | $Na_2SO_4$ | 24.4 | - | (30.8) |
| FiPOP | $Mg_2SO_4$ | 26.4 | - | (31.4) |

*Tab. 4: Dynamic modulus of elasticity $E_{\mathrm{DYN}}$*

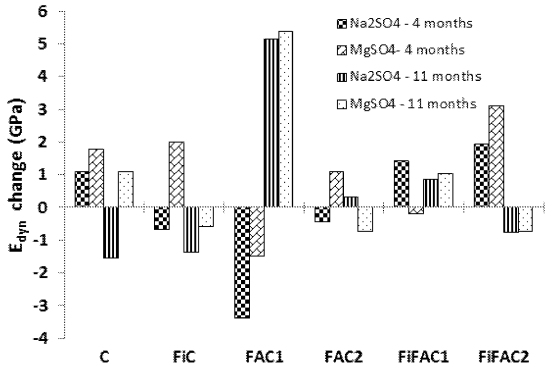


*Fig.4: Absolute change of $E_{\mathrm{DYN}}$ in relation to change in water*

## 4. Numerical simulation

This section offers the possibility of estimating the material parameters from fracture-mechanics tests by matching the experimentally measured and numerically derived loading curves. At the same, it raises a number of questions regarding the reliability of the results provided by either of the two methods if these are not mutually corroborated. The macroscopic loading curves of two selected concrete specimens denoted as C1 and C2 plotted in Fig. 7 as black solid lines were selected as our point of departure. Simulations performed in relation to fibrous specimens FiC1 and FiC2 appear in Fig. 8.

### 4.1. Static simulation of fracture energy test

To begin with, we adopted a simple trial and error method. The associated results stored in Table 5 are labeled as IDTE Mesh-TE where Mesh-TE denotes the finite element mesh seen in Fig. 5(a).

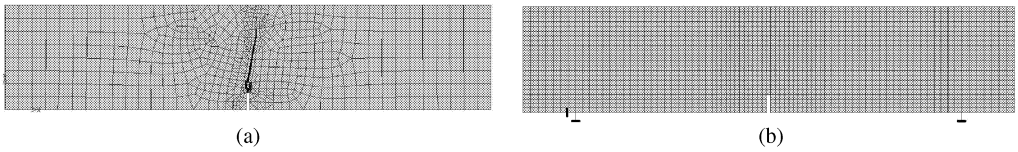


*Fig.5: Finite element meshes adopted in numerical simulations: (a) Mesh-TE, (b) Mesh-NN*

The ATENA finite element code [2] was used to simulate the three-point bending test numerically. A 3D Non Linear Cementitious 2 material model was selected to govern the gradual evolution of localized damage in fiber-free specimens. The model is formulated in the total format assuming small strains and initial isotropy of a material. The tensile behavior is governed by the Rankine-type criterion with exponential softening, while in compression the Menétrey-Willam yield surface with hardening and softening phases is used. The fracture model employs the orthotropic smeared crack formulation and the fixed crack model with the mesh adjusted softening modulus. This model is defined on the basis of characteristic element dimensions in tension and compression to ensure the objectivity in the strain-softening regime. The required material parameters are presented in Table 5.

| Parameter | IDTE Mesh-TE | IDNN Mesh-NN | IDNN Mesh-TE |
|---|---|---|---|
| Elastic modulus [GPa] | 48 / 55 | 82* / 96* | 82 / 96 |
| Poisson's number [-] | 0.2 | 0.2 | 0.2 |
| Tensile strength [MPa] | 3.8 / 4.5 | 2.7* / 2.9* | 2.7 / 2.9 |
| Compressive strength [MPa] | 72 | 72 | 72 |
| Specific fracture energy [N/m] | 70 / 60 | 228* / 206* | 228 / 206 |
| Specific weight [kN/m$^3$] | 24.7 | 24.7 | 24.7 |

*Tab.5: Material data of 3D Non Linear Cementitious 2 model for two specimens C1/C2 measured after 28 and 60 days of curing*

The material parameters employed in this case study are introduced in the first column of Table 5 (IDTE Mesh-TE). The objective was to use the experimentally obtained data if possible while attempting to match the available loading curves. While the Young's moduli and tensile strengths received only minor adjustment if compared with the measured values in Table 3, the specific fracture energy required a significant reduction to match measured and simulated loading curves reasonably close; compare the solid and dashed lines in Fig. 7. Compare also model fracture energies in the 1st column of Table 5 and the corresponding ones available in the last column (2nd row) of Table 3. These results are the first indication as to the inadequacy of the present fracture loading curves, recall Fig. 2, to extract, apart from specific fracture energies, other material data such e.g. the Young modulus or tensile strength. This issue will be addressed in the next section.

| Parameter | Data set 1 | Data set 2 | Data set 3 |
|---|---|---|---|
| Elastic modulus [GPa] | 48 / 55 | 48 / 55 | 27 |
| Poisson's number [–] | 0.2 | 0.2 | 0.2 |
| Tensile strength [MPa] | 3.8 / 4.5 | 2.0 / 2.4 | 2.7 |
| Compressive strength [MPa] | 72 | 72 | 72 |
| Specific fracture energy [N/m] | 70 / 65 | 100 / 65 | 100 |
| Specific weight [kN/m$^3$] | 23.0 | 23.0 | 23.0 |
| Fiber elastic modulus [GPa] | 1.45 | 1.45 | 1.45 |
| Fiber yield stress [MPa] | 150 | 150 | 150 |

*Tab.6: Material data of 3D Non Linear Cementitious 2 model for two specimens FiC1/FiC2*

To reproduce the fracture tests of fibrous specimens is not an easy task as a proper material model for a fiber reinforced concrete, taking into account all possible failure mechanisms including fiber pull-out, is not generally available in commercial codes. If, on the other hand, we are interested in the macroscopic response only it appears plausible to exercise the CCSmeardReinf material model implemented in the ATENA software to represent the smeared reinforcement. Such a model requires imputing the elastic modulus, yield stress, orientation and volume fraction of fibers. Since assuming a random distribution of fibers a quasi-isotropic lay-up of $0/90/\pm 45^\circ$ was considered with one quarter of the total volume fraction assigned to each fictitious ply. The remaining material data are available in Table 6. The resulting loading diagrams are shown in Fig. 8.

Again, the solid lines correspond to measured data. The remaining curves were constructed employing the Mesh-TE and the values of material parameters from Table 6. These were identified as before from a trial end error method exploiting the fiber yield stress as a free material parameter. It is seen that a reasonably close fit can be obtained when keeping the Young modulus and tensile strength relatively close to the experimentally derived data.

Note that the curve in Fig. 8(a) corresponding to the 3rd column in Table 6 was found when adjusting the Young modulus for the fitted curve to cross the experimental one at a theoretical yield stress of a concrete-fiber composite, see [13] for the definition of this variable. Unfortunately, the fitted specific fracture energy was found again way off the measured one. This issue will be addressed in the next section.

### 4.2. Numerical derivation of material data from inverse analysis

Quite severe deviations between measured and numerically estimated specific fracture energies provided by a simple direct approach promoted the application of a more rigorous type of inverse analysis adopting the elements of soft computing [3, 4]. Herein, we report on the approach combining artificial neural network (ANN) and finite element method.

Again the ATENA code was used to perform numerical simulations. The corresponding finite element mesh appears in Fig. 5(b). Based on sensitivity analysis [5] we considered Young's modulus $E$, tensile strength $f_{\mathrm{t}}$ and specific fracture energy $G_{\mathrm{f}}$ be subject to identification. These are labeled with (*) in Table 5. Other material data were assumed fixed either provided by experiment such as the compressive strength $f_{\mathrm{c,prism}}$ or assigned default values offered by the program for the selected material model. Attention was limited to concrete specimens.

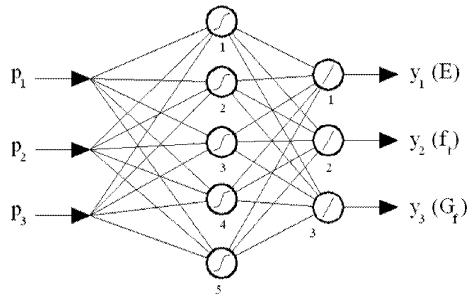


*Fig.6: Example of an artificial neural network*

As for the searching strategy, the implemented artificial neural network is of a feed-forward multilayer type. The network consisted of 3 inputs, one hidden layer having 5 neurons with non-linear transfer function (hyperbolic tangent) and output layer having 3 neurons with a linear transfer function, see Fig. 6. Each of the output neurons corresponds to one of the identified parameter. The size of training set was set to 50 samples generated using the Latin Hypercube Sampling method [7]. To train ANN Levenberg-Marquardt optimization method [8] and genetic algorithms [6] were used. Once ANN was trained the experimental response was used to obtain identified parameters. With this set of parameters numerical analysis was carried out and resulting response was compared with the experimental one. The resulting loading curves corresponding to identified parameters in Table 5 are plotted as solid lines with circle symbols (IDNN Mesh-NN) in Fig. 7.

Note that while the identified values of $G_{\mathrm{f}}$ are in a very good agreement with those provided by experiment, recall the 2nd row in Table 2, the identified values of Young's moduli are unrealistically high especially when compared to the measured ones. An independent experimental program is currently under way to reconcile this discrepancy and the results will be reported elsewhere. It has been observed that modifying some of the control parameters

in the experimental set up, e.g. the rate of loading, provides curves which yield the identified data close to the measured ones obtained from several independent tests, recall Section 3 and Table 3. This thus supports the measured specific fracture energies as material parameter applicable for structural analysis. Clearly, while acceptable for specific fracture energies the resulting curves from the present experiments (Section 3.1) can by no means be used to directly extract other material data such as the Young modulus and tensile strength.

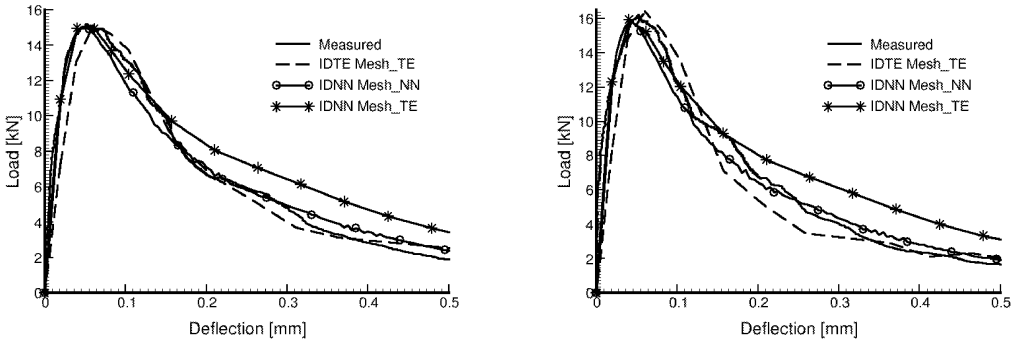


*Fig.7: Measured and numerically derived loading curves for two concrete specimens: (a) C1, (b) C2*

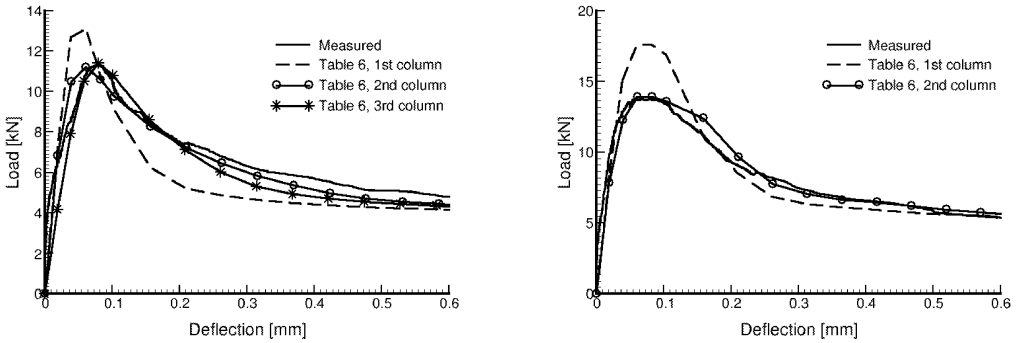


*Fig.8: Measured and numerically derived loading curves for two fiber concrete specimens: (a) FiC1, (b) FiC2*

There is still an open question as to the mesh dependent identification process, which one may ask when inspecting the solid lines with star symbols in Fig. 7 labeled as IDNN Mesh-TE. These were found after running the numerical analysis with identified data but adopting the unstructured coarse mesh in Fig. 5(a). It is reasonable to expect that for large scale structural analysis the adopted finite element mesh would be even coarser.

### 4.3. Dynamic simulation of fracture energy test

Learning from experience [11] a number of issues might be examined to provide solid explanation for inconsistency between experimental results and numerical simulations. The principal factor affecting the experimental results can be attributed to the relatively fast

rate of loading which should be reflected in numerical simulations by accounting for inertia properties of the components of loading test setup. Dynamic simulation of the crack propagation test discussed already by [10] can provide explanation to a high initial stiffness, recall the results of identification analysis, by incorporating the viscous damping of the specimen. This causes a slower stress distribution inside of the specimen and consequently leads to higher forces during fast loading. Other issues worth of future investigation include significant oscillations of time series of vertical displacements, unsymmetrical bending, etc.

## 5. Conclusions

The present contribution summarizes the experimental part of the project concerned with the modeling of TBM based tunneling in densely populated areas. Emphases were given to the experimental investigation of several cement and alkali activated fly ash based concrete mixtures. As was seen all concrete specimens complied with the strength requirements pertinent to tunnel lining. In addition, the specimens with a 30 % replacement of cement by fly ash performed nearly identically to cement only specimens. Even considerably higher amount of replaced cement up to 70 % should provide material with a sufficient strength and comparable performance. This issue is under current investigation. Finally, after 11 months under high sulphate solution no significant deterioration of samples was observed.

With principal attention paid to the specific fracture energy we attempted to confirm the experimental measurements by an independent numerical simulation of a three-point bending test employing the ATENA finite element code. Both simple trial and error method as well as more rigorous ANN based identification method were exercised. In the light of an ongoing independent study we confirm reliability of the experimentally derived specific fracture energies to be adopted as a material parameter in the constitutive model when performing a large analysis. On the other hand, the present loading curves cannot be used directly to extract other material parameters, Young's modulus and tensile strength, also provided by identification analysis. It has also been shown that fibrous samples can be well examined in the ATENA software employing the available constitutive model for a smeared reinforcement. To include the fiber yield stress as a free parameter in the identification analysis is the subject of our current research.

Attention also deserves a considerable dependence of the results of simulations on the finite element mesh promoting similar mesh coarseness used in lab experiments and structural simulations at least in areas prone to damage evolution.

## Acknowledgments

The financial support of the projects No. TA01030245 and No. TA01011019 provided by the Czech Technology Agency is gratefully acknowledged. We extend our personal thanks to Doc. Petr Bouška and Doc. Jiří Kolísko from the Klokner Institute in Prague for executing the experimental program.

## References

[1] Šmilauer V., Hlaváček P., Škvára F., Kopecký L., Němeček J.: Micromechanical multiscale model for alkali activation of fly ash and metakaolin, Journal of Material Sciece, Vol 46, No. 20, pp. 6545–6555, (2011)

[2] Červenka V., Jendele L., Červenka J.: ATENA Program Documentation – Part 1: Theory, Cervenka Consulting, Prague, Czech Republic, (2007)
[3] Novák D., Lehký D.: ANN Inverse Analysis Based on Stochastic Small-Sample Training Set Simulation, Engineering Application of Artificial Intelligence, Vol. 19, pp. 731–740, (2006)
[4] Lehký D., Novák D.: ANN Inverse Analysis in Stochastic Computational Mechanics, In: Artificial Intelligence: New Research, Berstein, (R.B., Curtis, W.N. eds), Nova Science Publishers, Hauppauge NY, USA, 323–350, (2009)
[5] Novák D., Teplý B., Shiraishi N.: Sensitivity analysis of structures: a review, In: 5th International Conference on Civil and Structural Engineering Computing, Edinburgh, Scotland, pp. 201–207, (1993)
[6] Haupt R.L., Haupt S.E.: Practical Genetic Algorithms, John Wiley Sons, Inc., Hoboken, New Jersey, USA, (2004)
[7] McKay M.D., Conover W.J., Beckman R.J.: A comparison of three methods for selecting values of input variables in the analysis of output from a computer code, Technometrics, Vol. 21, pp. 239–245, (1979)
[8] Singh V., Gupta I., Gupta H.O.: ANN-based estimator for distillation using Levenberg-Marquardt approach, Engineering Applications of Artificial Intelligence, Vol. 20, pp. 249–259, (2007)
[9] Frantík P., Pruša J., Keršner Z., Macur J.: About stability loss during displacement-controlled loading, In: Fiber Concrete 2007, September 12–13, Prague, Czech Republic, (2007)
[10] Frantík P.: Czech Dynamic simulation of crack propagation experiments, In: Engineering Mechanics 2008, May 12–15, Svratka, Czech Republic, (2008)
[11] Keršner Z., Lehký D., Novák D., Kucharczyková B., Frantík P., Bedáň J.: Fracture Energy Tests: Specimens (C30/37 H), II (C25/30 B3), III (C25/30 XC1 GK16), IV (C20/25 XC1 GK16), Internal Report, Brno University of Technology, Faculty of Civil Engineering, Institute of Structural Mechanics and Institute of Building Testing, (2011)
[12] RILEM: Technical Recommendations for the Testing and Use of Construction Materials, London: F&FN
[13] ČSN EN 14651+A1: Test method for metallic concrete – Measuring the flexural tensile strength (limit of proportionality (LOP), residual), CEN, Brusel

*Received in editor's office*: October 1, 2012
*Approved for publishing*: February 24, 2014